Published in final edited form as:
Sci Signal. ; 6(286): ra64. doi:10.1126/scisignal.2004111.

Phosphatidylcholine Transfer Protein Interacts with Thioesterase Superfamily Member 2 to Attenuate Insulin Signaling

Baran A. Ersoy[1], **Akansha Tarun**[1], **Katharine D'Aquino**[2], **Nancy J. Hancer**[2], **Chinweike Ukomadu**[1], **Morris F. White**[2], **Thomas Michel**[1], **Brendan D. Manning**[3], and **David E. Cohen**[1,*]

[1]Department of Medicine, Brigham and Women's Hospital, Harvard Medical School, Boston MA 02115

[2]Howard Hughes Medical Institute, Division of Endocrinology, Children's Hospital Boston, Harvard Medical School, Boston, MA 02115

[3]Department of Genetics and Complex Diseases, Harvard School of Public Health, Boston, MA 02115

Abstract

Phosphatidylcholine transfer protein (PC-TP) is a phospholipid-binding protein that is enriched in liver and that interacts with thioesterase superfamily member 2 (THEM2). Mice lacking either protein exhibit improved hepatic glucose homeostasis and are resistant to diet-induced diabetes. Insulin receptor substrate 2 (IRS2) and mammalian target of rapamycin complex 1 (mTORC1) are key effectors of insulin signaling, which is attenuated in diabetes. We found that PC-TP inhibited IRS2, as evidenced by insulin-independent IRS2 activation following knockdown, genetic ablation, or chemical inhibition of PC-TP. In addition, IRS2 was activated after knockdown of THEM2, providing support for a role for the interaction of PC-TP with THEM2 in suppressing insulin signaling. Additionally, we showed that PC-TP bound to tuberous sclerosis complex 2 (TSC2) and stabilized the components of the TSC1-TSC2 complex, which functions to inhibit mTORC1. Preventing phosphatidylcholine from binding to PC-TP disrupted interactions of PC-TP with THEM2 and TSC2, and disruption of the PC-TP–THEM2 complex was associated with increased activation of both IRS2 and mTORC1. In livers of mice with genetic ablation of PC-TP or that had been treated with a PC-TP inhibitor, steady-state amounts of IRS2 were increased, whereas those of TSC2 were decreased. These findings reveal a phospholipid-dependent mechanism that suppresses insulin signaling downstream of its receptor.

[*]To whom correspondence should be addressed: Brigham and Women's Hospital, 77 Avenue Louis Pasteur, HIM Building Room 941, Boston, MA 02115. Tel: 617-525-5090; Fax: 617-525-5100; dcohen@partners.org.

Supplementary Materials

Fig. S1. Roles of PI3K, mTORC2, PTEN, oxidative stress, PKA, MAPK, PLC and AMPK in the inhibition of Akt activity by PC-TP and THEM2

Fig. S2. Inhibition of IRS2 by PC-TP

Fig. S3. Characterization of a mouse antibody to phosphorylated IRS2 at Ser^{924}

Fig. S4. Compound A1-mediated disruption of PC-TP interactions with THEM2 and TSC2

Fig. S5. Inhibition of TSC2 phosphorylation by PC-TP and THEM2

Author contributions: BAE, CU, MFW, TM, BDM and DEC designed experiments. BAE, AT, KD and NJH collected data. BAE, CU, MFW, TM, BDM and DEC analyzed data. BAE, TM, BDM and DEC wrote the manuscript.

Competing interests: The authors declare that they have no competing interests.

Introduction

Phosphatidylcholine transfer protein (PC-TP; also known as StARD2) is a liver-enriched cytosolic lipid binding protein that belongs to the steroidogenic acute regulatory transfer-related (START) domain superfamily. PC-TP was initially characterized as a protein that catalyzes the intermembrane exchange of phosphatidylcholines *in vitro* (1). Its highly selective lipid binding pocket accommodates a single phosphatidylcholine molecule and preferentially binds phosphatidylcholines with more unsaturated sn-2 fatty acyl chains (1–3), which may in turn influence the conformation of PC-TP (4). By mechanisms that appear to be distinct from lipid transfer activity, PC-TP reduces hepatic insulin sensitivity. In chow fed *Pctp*$^{-/-}$mice, decreased fasting plasma glucose concentrations are accompanied by reduced hepatic glucose production in hyperinsulinemic-euglycemic clamp studies (6). *Pctp*$^{-/-}$mice are also resistant to diet-induced diabetes, and treatment with a small molecule inhibitor of PC-TP improves glucose tolerance and reduces hepatic glucose production in wild-type mice (7). Coding region polymorphisms have also been reported in both mice (8) and humans (9), which appear to confer protection against insulin resistance (4). Improvements in glucose homeostasis are associated with enhanced hepatic insulin signaling through an unknown mechanism. In the absence of PC-TP or in response to its chemical inhibition, livers and primary hepatocytes exhibit increased phosphorylation of Akt and its downstream targets (6, 7).

PC-TP interacts with thioesterase superfamily member 2 (THEM2) (10), a soluble homotetrameric fatty acyl-CoA thioesterase (also known as ACOT13) (11). Like PC-TP, THEM2 is enriched in liver, is a transcriptional target of peroxisome proliferation-activated receptor α (PPARα) and reversibly associates with mitochondria (2, 5, 11). As observed for PC-TP-deficient mice, *Them2*$^{-/-}$mice exhibit phenotypes that include reduced hepatic glucose production and resistance to diet-induced diabetes (12). The enzymatic activities of both purified recombinant THEM2 and PC-TP are increased by their interaction (10, 11), but the biological relevance of this effect is unknown.

To elucidate molecular mechanisms that may underlie improved glucose homeostasis in *Pctp*$^{-/-}$mice, we examined the regulation of insulin signaling by PC-TP in cell culture systems and *in vivo*. Insulin binding to its receptor activates insulin receptor substrate (IRS) proteins, which promote phosphoinositide 3-kinase (PI3K)- and 3-phosphoinositide-dependent kinase (PDK1)-mediated phosphorylation of Akt at Thr^{308} (13, 14). Full activation of Akt requires additional phosphorylation at Ser^{473}, which is mediated by mammalian target of rapamycin (mTOR) complex 2 (mTORC2) (15). Among the downstream targets of phosphorylated Akt are AMPK (16), GSK-3β (17) and tuberous sclerosis complex 2 (TSC2) (18). The TSC1-TSC2 complex inhibits mTORC1 and its targets, including S6K1 (19).

siRNA-mediated knockdown, genetic ablation or chemical inhibition of PC-TP increased insulin signaling by enhancing insulin-independent activation of IRS2, with knockdown of THEM2 yielding similar effects. PC-TP and THEM2 also suppressed mTORC1 signaling upon binding TSC2. Chemical inhibition of PC-TP to prevent phosphatidylcholine binding (7) disrupted the interactions of PC-TP with THEM2 and TSC2. Our findings reveal a phospholipid-dependent mechanism for suppressing insulin signaling: a PC-TP-THEM2 complex reduces phosphorylation and stability of IRS2 and increases stability of the TSC1-TSC2 complex.

Results

Inhibition of the activity of Akt and its key targets by PC-TP and THEM2

In serum-starved HEK 293E cells, knockdown of THEM2 was associated with a 50% reduction in PC-TP abundance, whereas knockdown of PC-TP tended to increase THEM2 abundance (Fig. 1, A and B). We next determined whether PC-TP and THEM2 influenced the activity of Akt and its key targets. In the absence of insulin, siRNA-mediated knockdown of either PC-TP or THEM2 resulted in 2- and 3-fold increases in the phosphorylation of Akt at Ser^{473}, a 30% decrease in the phosphorylation of AMPK for either condition, and 3- and 6-fold increases in the phosphorylation of S6K1, respectively (Fig. 1, A and C). Phosphorylation of GSK-3β was increased 2-fold after PC-TP or THEM2 knockdown, although these effects did not achieve statistical significance. In response to insulin, the increased phosphorylation of Akt at both Ser^{473} and Thr^{308} was additive to the increase in basal activation of Akt (Fig. 1D).

Because the 48 h time frame for PC-TP knockdown allowed for the possibility that effects on Akt activation were secondary to adaptive transcriptional or metabolic effects, we used compound A1, a small molecule inhibitor that rapidly inactivates PC-TP and increases the phosphorylation of Akt, S6K1, and GSK-3β in primary human hepatocytes (7). Short-term (30 min) treatment with compound A1 (Fig. 1E) increased the phosphorylation of Akt in primary hepatocyte cultures from $Pctp^{+/+}$ mice but not in those from $Pctp^{-/-}$mice. Chemical inhibition of PC-TP was associated with slight increases in the abundance of PC-TP (Fig. 1E). As observed for PC-TP knockdown in HEK 293E cells (Fig. 1D), the effect of chemical inhibition of PC-TP on Akt was additive to insulin in $Pctp^{+/+}$ hepatocytes (Fig. 1F).

Phosphatidylinositol-3 kinase (PI3K)-dependent suppression of Akt activity by PC-TP and THEM2

We utilized chemical inhibitors to ascertain a role for PI3K in the regulation of Akt by PC-TP and THEM2 (Fig. 2A and Fig. S1A). Wortmannin reduced phosphorylation of Akt by 84% in HEK 293E cells treated with scrambled siRNA, but only by 50% following knockdown of PC-TP or THEM2 (Fig. 2A, inset bar graph). Because high concentrations of wortmannin can inhibit phosphorylation of Akt by reducing the activity of mammalian target of rapamycin complex (mTORC) 2 (15), we also measured IC_{50} values for GDC-0941, which provided quantitative measures of responsiveness of Akt phosphorylation to PI3K inhibition. Compared with scrambled siRNA, knockdown of PC-TP and THEM2 increased the IC_{50} values for GDC-0941-mediated inhibition of Akt phosphorylation by 3.2- and 5.7-fold, respectively (Fig. S1A, inset plots). Knockdown of PC-TP or THEM2 also decreased the extent to which Akt activity was suppressed by the highest dose of GDC-0941 (Fig. S1A, inset plots). However, we limited GDC-0941 concentrations to ≤ 100 nM because higher concentrations can result in PI3K-independent inhibition of Akt (20). For higher GDC-0941 concentrations, we measured cellular phosphatidylinositol 3,4,5-trisphosphate (PIP_3) concentrations as a marker of PI3K activity. PC-TP and THEM2 knockdown increased PIP_3 concentrations by 1.7- and 2.3-fold, respectively (Fig. 2B). Furthermore, the IC_{50} values for GDC-0941-mediated reductions in PIP_3 concentrations (Fig. 2C) were increased 10-fold and 3-fold following siRNA-mediated knockdown of PC-TP and THEM2, respectively (Fig. 2C, inset plot), providing further evidence of PI3K-dependent regulation. Wortmannin treatment, which blocked Akt activation by PC-TP or THEM2 knockdown, also abrogated the reduction in the phosphorylation of AMPK (Fig. 2A), thus showing that reduced AMPK activation in response to knockdown of PC-TP or THEM2 (Fig. 1, A and C) was secondary to the activation of Akt and not a distinct mechanism by which PC-TP inhibits mTORC1 signaling.

Unexpectedly, wortmannin did not reduce the phosphorylation of S6K1 (Fig. 2A). S6K1 is phosphorylated by mTORC1 (21), and mTORC1 inhibition by rapamycin suppressed the phosphorylation of S6K1 in HEK 293E cells after knockdown of PC-TP or THEM2, but did not suppress the activation of Akt (Fig. 2D). We validated this effect in the setting of acute PC-TP or mTORC1 inhibition (Fig. 2, E and F). In HEK 293E cells or primary hepatocytes from *Pctp*$^{+/+}$ mice, rapamycin treatment increased the basal phosphorylation of Akt; however, compound A1 treatment did not result in further induction of Akt phosphorylation (Fig. 2, E and F). At the highest dose of compound A1, phosphorylation of Akt at Thr^{308} was reduced in HEK 293E cells. This dose likely resulted in potent or sustained activation of insulin signaling and PI3K, which would be expected to lead to S6K1-mediated negative feedback and suppression of further stimulation of 3-phosphoinositide dependent protein kinase-1 (PDK1) (22, 23), the kinase that targets Akt at Thr^{308} (24).

We also tested the effects of silencing PC-TP and THEM2 on other mechanisms for Akt activation. mTORC2 activates Akt by phosphorylating it at Ser^{473} (15), and knockdown of PC-TP or THEM2 diminished mTORC2 activity in an *in vitro* assay (15), as evidenced by reduced phosphorylation of an exogenous inactive Akt substrate at Ser^{473} (Fig. S1B). This occurred independently of the induction of the phosphorylation of Ser^{473} in cell lysates (Fig. S1B). In addition, siRNA-mediated knockdown of phosphatase and tensin homolog (PTEN) (25) increased Akt activity but did not eliminate the increased phosphorylation of Akt after PC-TP or THEM2 knockdown (Fig. S1C). Similarly, the induction of oxidative stress by hydrogen peroxide (H_2O_2) treatment (26) did not alter increased phosphorylation of Akt after knockdown of PC-TP or THEM2 (Fig. S1D). Inhibition of protein kinase A (PKA) by H89 resulted in increased basal phosphorylation of Akt and S6K1, but increases due to PC-TP and THEM2 knockdown persisted (Fig. S1E). Inhibition of mitogen-activated protein kinase (MAPK) by PD98059, phospholipase C (PLC) by U73122, or AMPK by the Ca^{2+}/calmodulin-dependent protein kinase kinase β (CaMKKβ) inhibitor STO-609 had no appreciable effect on either basal phosphorylation of Akt and S6K1 or the activation of Akt after PC-TP or THEM2 knockdown (Fig. S1, E and F). Taken together, these findings argue against a role for mTORC2, PTEN, oxidative stress, PKA, MAPK, PLC, or AMPK in the activation of Akt that occurs after knockdown of PC-TP or THEM2.

Key role for IRS2 in the inhibition of PI3K by PC-TP and THEM2

In our search for a potential mechanism for the PI3K-dependent inhibition of Akt by PC-TP and THEM2, we were guided by our prior observation that *IRS2* mRNA expression was increased in livers of *Pctp*$^{-/-}$mice (6). In HEK 293E cells, the protein abundance of IRS2 was increased after knockdown of either PC-TP or THEM2 (Fig. 3, A and B), whereas that of IRS1 was unchanged (Fig. S2A). Steady state *IRS2* mRNA abundance were increased following PC-TP knockdown and tended to increase following THEM2 knockdown (Fig. 3B). IRS proteins are activated by phosphorylation at Tyr residues (27, 28). Because Tyr phosphorylation of IRS2 was also increased after PC-TP and THEM2 knockdown (Fig. 3C), the effects of PC-TP and THEM2 on IRS2 most likely reflected both transcriptional and post-transcriptional regulation. Knockdown of IRS2 abrogated the induction of phosphorylation of Akt at Thr^{308} and Ser^{473} caused by knockdown of PC-TP or THEM2 (Fig. 3, A and D). IRS2 stimulates Akt activity by increasing cellular PIP_3 production (29), and the increases in PIP_3 accumulation after knockdown of PC-TP or THEM2 were eliminated by concurrent knockdown of IRS2 (Fig. 3E).

To explore the relative contribution of post-transcriptional regulation to Akt activation, we examined the effect of compound A1 on the abundance and activation of IRS2. Short-term treatment with compound A1 led to increased IRS2 protein abundance in *Pctp*$^{+/+}$ but not *Pctp*$^{-/-}$hepatocytes (Fig. 3F), which was most likely attributable to a post-transcriptional

mechanism because *IRS2* mRNA abundance was not affected (Fig. 3G). In contrast, compound A1 increased the mRNA abundance for PC-TP, presumably because of a transcriptional response to chemical inactivation (Fig. 3G). Knockdown of PC-TP increased the half-life ($t_{1/2}$) for IRS2 protein by 1.9-fold (Fig. S2, B and C). Prolonged exposure of HEK 293E cells to compound A1 also reduced the electrophoretic mobility of IRS2, presumably reflecting increased phosphorylation (Fig. S2, D and E), and decreased the steady state abundance of IRS2 protein (Fig. S2F). Tyr phosphorylation, including at Tyr^{911}, was increased in $Pctp^{+/+}$ hepatocytes by treatment with compound A1 (Fig. 3H and Fig. S2, G and H). In addition, inhibition of IRS2 may have been reduced by compound A1, as evidenced by a 68% decrease in phosphorylation of Ser^{924} (Fig. S2, G and H) using a site-specific antibody (Fig. S3, A to C). Because Ser phosphorylation has been implicated in the inhibition of IRS2 (27, 28), inhibition of Ser^{924} phosphorylation by compound A1 may have contributed to the observed increase in the activities of IRS2 and Akt.

Stabilization of the TSC1-TSC2 protein complex by PC-TP and THEM2

We next explored the mechanism by which PC-TP and THEM2 induced the phosphorylation of S6K1 independently of that of Akt (Fig. 2A). Because the TSC1-TSC2 complex inhibits mTORC1-mediated phosphorylation of S6K1 (30, 31), we revisited our previous observation from a yeast-two hybrid screen (32), which suggested a direct interaction between PC-TP and TSC2. We verified this interaction with both GST pulldown and co-immunoprecipitation assays (Fig. 4). Endogenous TSC2 in lysates of HEK 293E cells interacted with a GST-PC-TP fusion protein but not GST alone (Fig. 4A). Endogenous TSC1 also co-precipitated with GST-PC-TP and TSC2 (Fig. 4A). To further validate the identity of TSC2 in the pulldown assays, we utilized $Tsc2^{-/-}$and $Tsc2^{+/+}$ MEFs: Only endogenous TSC2 from $Tsc2^{+/+}$ MEF lysates yielded a band for TSC2 following GST-PC-TP pulldown (Fig. 4B). In addition, both TSC1 and TSC2 co-immunoprecipitated with PC-TP from HEK 293E cells expressing FLAG-tagged TSC1 and TSC2 along with Myc-tagged PC-TP (Fig. 4C). Finally, endogenous TSC2 coimmunoprecipitated with PC-TP from liver lysates from $Pctp^{+/+}$ mice (Fig. 4D).

Next we utilized GST pulldown assays to examine whether compound A1 might disrupt the interactions among PC-TP, THEM2 and TSC2. Compound A1 reduced PC-TP-THEM2 interactions, as reflected by decreased pulldown of endogenous THEM2 in HEK 293E cells by GST-PC-TP (Fig. S4A). Compound A1 also disrupted the interaction between PC-TP and TSC2 (Fig. S4B), providing further evidence that the PC-TP-THEM2 complex stabilized the TSC1-TSC2 complex.

Knockdown of either PC-TP or THEM2 reduced the steady state abundance of TSC2 (Fig. 4E) but not *TSC2* mRNA abundance (Fig 4F). This observation was supported by measurements of protein turnover rates following knockdown of THEM2 (Fig. 4, G and H): Half-life values were reduced 5.6-fold for TSC2 and 3.5-fold for TSC1. The $t_{1/2}$ of PC-TP was reduced by 2.9-fold following THEM2 knockdown, which presumably explains the reduction in PC-TP abundance following THEM2 knockdown (Fig. 1B).

Because Akt phosphorylates TSC2 on Thr^{1462} (18), we also examined the effect of PC-TP and THEM2 on the phosphorylation of TSC2. Knockdown of either PC-TP or THEM2 resulted in increased phosphorylation of TSC2 (Fig. S5A). However, it was uncertain whether Akt was responsible for this phosphorylation because the PI3K inhibitor GDC-0941 reduced the phosphorylation of Akt but not that of TSC2 (Fig. S5A). Inhibition of PC-TP by compound A1 also resulted in increased phosphorylation of TSC2 and S6K1 and increased abundance of IRS2 (Fig. S5B), the latter of which was not further increased by rapamycin treatment.

Reduced PC-TP and THEM2 turnover but preserved IRS2 responsiveness in *Tsc2*$^{-/-}$MEFs

We used *Tsc2*$^{-/-}$and *Tsc2*$^{+/+}$ MEFs to determine the role of TSC2 in the regulation of PC-TP and THEM2 (Fig. 5). Although the abundance of THEM2 was similar in both types of MEFs, PC-TP abundance was greater in *Tsc2*$^{-/-}$MEFs than in *Tsc2*$^{+/+}$ MEFs, which had almost undetectable amounts of PC-TP (Fig. 5A), consistent with prior observations in a rat fibroblast cell line (33). When TSC2 was reintroduced into *Tsc2*$^{-/-}$MEFs by transient transfection, the endogenous steady state protein abundance of PC-TP decreased markedly (Fig. 5A), whereas steady state *PC-TP* mRNA abundance remained unchanged (Fig. 5B). TSC2 transfection reduced the $t_{1/2}$ of PC-TP by 2.0-fold (Fig. 5, C and D) and that of THEM2 by 9.7-fold, but the stability of TSC1 was not altered appreciably (Fig. 5, C and D).

As observed in HEK 293E cells (Fig. 1), THEM2 knockdown in both *Tsc2*$^{-/-}$and *Tsc2*$^{+/+}$ MEFs increased the phosphorylation of Akt (Fig. 5E). In *Tsc2*$^{+/+}$ MEFs, phosphorylation of S6K1 was also increased upon THEM2 knockdown. Phosphorylation of S6K1 was robustly increased in *Tsc2*$^{-/-}$MEFs, an effect that was modestly reduced following THEM2 knockdown (Fig. 5E). In *Tsc2*$^{-/-}$MEFs, knockdown of PC-TP or THEM2 increased both IRS2 protein abundance and phosphorylation of Akt (Fig. 5F), suggesting that IRS2-mediated Akt activation was independent of mTOR activity.

Increased IRS2 and reduced TSC2 abundance in livers of mice following genetic ablation or chemical inhibition of PC-TP

To confirm that inhibition of insulin signaling by PC-TP occurred *in vivo*, we examined the hepatic responses of *Pctp*$^{-/-}$and *Pctp*$^{+/+}$ mice to fasting or to treatment with compound A1. In response to food withdrawal, chow fed *Pctp*$^{-/-}$mice exhibited a 3.7-fold induction in IRS2 abundance whereas that of IRS1 remained unchanged (Fig. 6, A and B). Phosphorylation of Akt and S6K1 were increased 2.8- and 3.1-fold, respectively, in the livers of *Pctp*$^{-/-}$mice compared to *Pctp*$^{+/+}$ mice (Fig. 6, A and C). Although these changes did not achieve significance, PC-TP deficiency also reduced TSC2 abundance by 35% (Fig. 6, A and B) and increased TSC2 phosphorylation by 5.4-fold (Fig. 6, A and C).

We previously demonstrated that compound A1 treatment reduces hepatic glucose production, while increasing phosphorylation of Akt and S6K1 in livers of *Pctp*$^{+/+}$ but not *Pctp*$^{-/-}$mice on a high-fat diet (7). Further analysis of these mouse livers revealed that compound A1 treatment of *Pctp*$^{+/+}$ mice increased IRS2 abundance by 2.1-fold and reduced steady state TSC2 abundance by 47% (Fig. 6, D and E). Similar to what was observed in isolated hepatocytes (Fig. 3, F and G), compound A1 treatment also led to a 58% increase in PC-TP abundance (Fig. 6, D and E), most likely as a compensatory response. Phosphorylation of Akt and S6K1 was increased 6.6- and 3.2-fold, respectively (Fig. 6, D and F), effects that were consistent with the *in vitro* effects of compound A1 (Fig. S5B).

Discussion

This study has revealed regulatory functions of PC-TP and THEM2 in the control of cellular insulin signaling. Taken together, our observations support a model (Fig. 7) in which a complex of PC-TP and THEM2 suppresses the activation of IRS2 and mTORC1 in response to binding to membrane phosphatidylcholines. In support of a functional PC-TP-THEM2 complex, knockdown of either protein yielded similar effects on both IRS2 and mTORC1 activity. Reduced PC-TP protein abundance after knockdown of THEM2 also indicated that PC-TP was more stable when complexed with THEM2.

PC-TP-dependent attenuation of Akt activity required IRS2. PC-TP inhibition increased the activity of IRS2, as indicated by enhanced Tyr^{911} phosphorylation and reduced

phosphorylation at Ser^{924}. Because Tyr^{911} is the putative binding site on IRS2 for GRB2 (growth factor receptor-bound protein 2) (34) and Ser^{924} resides within an extracellular signal-regulated kinase (ERK) phosphorylation motif (Ser/ThrPro) (35), these findings suggest mechanisms by which PC-TP may inhibit IRS2. Whereas the absence of increased IRS2 abundance in response to compound A1 following rapamycin treatment might have implied a role for mTORC1, rapamycin-induced increases also occurred in IRS2 in the absence of compound A1.

In the setting of PC-TP and THEM2 knockdown, the increased abundance of *IRS2* mRNA also suggested a distinct mTOR-independent transcriptional mechanism. A possible explanation includes the transcription factor sterol regulatory element binding protein 1c (SREBP-1c), which is activated by increased cellular nutrition and energy availability (36). Inhibition of IRS2 transcription by SREBP-1c in response to excess energy (36) is a plausible mechanism because livers of fasted $Pctp^{-/-}$mice showed increased mRNA abundance of *IRS2* concurrent with reduced mRNA abundance of SREBP-1c (6).

Although transcriptional activation of *IRS2* in response to PC-TP and THEM2 knockdown did not directly depend upon mTOR activity, our findings nevertheless suggest that key aspects of mTOR activity were controlled by interactions between these two proteins and TSC2. The TSC1-TSC2 complex inhibits mTOR signaling (37, 38). Because TSC1 stabilizes TSC2, disruption of the TSC1-TSC2 complex leads to rapid degradation of TSC2 (39). Accordingly, THEM2 knockdown resulted in similar decreases in the $t_{1/2}$ of TSC1 and TSC2 and in the activation of mTORC1. Heterologous expression of TSC2 in $Tsc2^{-/-}$MEFs to reconstitute the TSC1-TSC2 complex increased the turnover rates of PC-TP and THEM2. This suggests that PC-TP and THEM2, which stabilize the TSC1-TSC2 complex, were in turn destabilized by the same protein complex, potentially in response to changes in mTORC1 signaling. Alternatively plasmid-mediated expression of excess TSC2 in relation to endogenous TSC1 could have resulted in rapid degradation of PC-TP, THEM2 and TSC2, which is unstable when not bound by TSC1 (39). Additional studies will be required to discern whether regulation of mTOR signaling by PC-TP and THEM2 is mechanistically related to the transcriptional control of IRS2 or whether this results in other as yet uncharacterized metabolic effects.

A key objective of this study was to gain insights into mechanisms of improved glucose homeostasis exhibited by $Pctp^{-/-}$and $Them2^{-/-}$mice (6, 12) and following chemical inhibition of PC-TP in wild-type mice on a high-fat diet (7). Although initially characterized *in vitro* as a protein with lipid transfer activity (1), we have proposed that PC-TP may instead function as a sensor of membrane phosphatidylcholines (4), such that changes in membrane composition that accompany feeding or fasting are reflected in the molecular species of phosphatidylcholines bound to PC-TP. These may in turn promote PC-TP interactions with THEM2 and TSC2 through phosphatidylcholine-mediated conformational changes. This possibility is supported by the mechanism of inhibition of PC-TP by compound A1, which binds and displaces phosphatidylcholines from the lipid binding site (7), thereby increasing the thermal stability of the protein (7) and disrupting its interaction with THEM2 and TSC2. These findings suggest that phospholipid binding to PC-TP suppresses insulin signaling by interactions with THEM2 and TSC2. In support of this model and consistent with prior *in vivo* evidence for activation of insulin signaling following genetic ablation or pharmacological inhibition of PC-TP in mice (6, 7), the current study demonstrated increased hepatic IRS2 abundance and decreased TSC2 abundance in livers of both $Pctp^{-/-}$mice and mice treated with compound A1. When taken together, these findings reveal a phospholipid-mediated mechanism that controls insulin signaling (Fig. 7).

Experimental Procedures

Reagents

Cell culture media and supplies were purchased from Invitrogen (Carlsbad, CA). Wortmannin, rapamycin, STO-609, H89 and PD98059 were from EMD Chemicals (Gibbstown, NJ). U73122 was from Enzo Life Sciences (Plymouth Meeting, PA). GDC-0941 was from Chemdea (Ridgewood, NJ). Insulin and cycloheximide were from Sigma-Aldrich (St. Louis, MO). Protein A Dynabeads were from Invitrogen, and glutathione-Sepharose 4B beads were from GE Healthcare (Piscataway, NJ). The PC-TP inhibitor compound A1 (4-[3-(2,4-dichlorobenzoyl)ureido]-N-(4,6-dimethylpyrimidin-2-yl)benzenesulfonamide) was synthesized as previously described (7). Polyclonal antibodies to PC-TP and THEM2 were prepared as previously described (10). Antibodies to most total and phosphorylated proteins were from Cell Signaling Technology (Danvers, MA). A total GSK-3β antibody was from BD Transduction Laboratories (Woburn, MA). Antibodies to TSC2 (tuberin C-20) and p-Tyr, as well as rabbit IgG were from Santa Cruz Biotechnology (Santa Cruz, CA). A mouse monoclonal antibody to β-Actin was from Sigma-Aldrich. An antibody to IRS1 (pre CT) was from Upstate (Lake Placid, NY).

Cell culture and transfection

Tsc2$^{+/+}$ and *Tsc2*$^{-/-}$ (both *p53*$^{-/-}$) mouse embryonic fibroblasts (MEFs) and human embryonic kidney (HEK) 293E cells (40) were cultured in Dulbecco's modified Eagle's medium (DMEM) supplemented with 10% (v/v) fetal bovine serum (FBS) (Invitrogen). A cDNA encoding human PC-TP was cloned into a pCMV-myc plasmid (Clontech, Mountain View, CA) using EcoR1 and Xho1 (Invitrogen), which introduced a c-myc tag in frame at the N-terminus of the protein. Wild-type human *Tsc1* and *Tsc2* cDNAs were cloned so that a FLAG tag was fused to the N-termini as previously described (30). Transient transfection of plasmids was performed using Effectene transfection reagent (Qiagen, Valencia, CA) according to the manufacturer's protocol. Cells at 50% confluence in DMEM-10% FBS (220μl final volume/cm^2 of culture vessel surface area) were transfected with plasmids (0.2 μg/ml) and experiments were conducted 48 h following transfection.

An siRNA targeting human PC-TP corresponded to nt 246–264 of the open reading frame: 5′-CCAGUAUGUUAAAGAACUCtt-3′ (ID 121081, Ambion, Austin, TX). An siRNA targeting human THEM2 corresponded to nt 411–423 from the open reading frame plus 6 nucleotides of the 3′ UTR following the stop codon: 5′-CCUGGGAAACUGAGAGAACtt-3′ (ID 119801, Ambion). An siRNA targeting human IRS2 corresponded to nt 2750–2768 of the open reading frame: 5′-GCGAGUACAUCAACAUCGAtt-3′ (ID s16488, Ambion). An siRNA targeting human PTEN corresponded to nt 388–406 of the open reading frame: 5′-CGAACUGGUGUAAUGAUAUtt-3′ (ID 114050, Ambion). A control scrambled siRNA (AM4611) was also from Ambion. siRNAs were transfected using Lipofectamine 2000 reagent (Invitrogen) according to the manufacturer's protocol. Preliminary experiments established that optimal knockdown was achieved using 30 nM siRNA and 0.2% Lipofectamine 2000. Transfection complexes were prepared in Opti-MEM Reduced Serum Medium (Invitrogen) without serum. Cells at 50% confluence in DMEM-10% FBS (200 μl/cm^2 of culture vessel surface area) were transfected. The media was replaced with DMEM-10% FBS 6 h following transfection and DMEM 40 h following transfection, and experiments were conducted 48 h after transfection. All experiments were conducted following 8 h serum-starvation. Cells were incubated with 0.01–10 μM compound A1 for 30 min unless otherwise specified. Cells were treated with 1–100 nM insulin, 1–100 nM GDC-0941, 20 nM rapamycin, 100 μM H_2O_2, 10 μM H89, 50 μM PD98059, 10 μM U73122 or 10 μM STO-609 for 30 min, whereas 100 nM wortmannin was added for 15 min.

For all treatments, the control vehicle was DMSO, with the exception that PBS was the vehicle for H_2O_2 delivery. EC_{50} and IC_{50} values for activation and inhibition of phosphorylation of Akt, respectively, were calculated from densitometric analyses by non-linear least square analysis using Prism 4 (GraphPad Software, La Jolla, CA).

Mouse studies

Male *Pctp*$^{+/+}$ and *Pctp*$^{-/-}$mice 7 generations backcrossed into FVB/NJ background (41) were housed in a standard 12 h alternate light/dark cycle and fed a standard rodent diet 5001 (LabDiets, St. Louis, MO, USA) with free access to drinking water. Mouse primary hepatocytes were isolated and cultured as previously described (6). Briefly, mice were anesthetized with an i.p. injection of ketamine (200 mg/kg body weight; Webster Veterinary, Sterling, MA) plus xylazine (15 mg/kg body weight; Webster Veterinary). The inferior vena cava was exposed, cannulated, and perfused with 20 ml of liver perfusion media (Invitrogen), followed by 30 ml of liver digestion media (Invitrogen), both kept at 37 °C. The portal vein was severed in order to provide an exit route for the perfusate. The digested liver was removed, minced with a surgical blade in 10 ml of ice cold hepatocyte wash media (Invitrogen), passed through a 70 micron filter (BD Biosciences, San Jose, CA), pelleted by gentle centrifugation (50 × g for 2 min) and washed 3 times with 50 ml ice-cold hepatocyte wash media. Cells were then resuspended in cold (4 °C) Williams E medium (Invitrogen) containing 10% FBS, 1 μM dexamethasone and 20 ng/ml EGF. Viability was estimated by the trypan blue exclusion, and cells were plated on Primaria plates (BD Biosciences) at 80% confluence. After 24 h, hepatocytes were washed with PBS, and the culture media was replenished. Thirty six h following plating, the cells were washed with PBS and serum starved in plain Williams E medium overnight. Experiments were performed 48 h after plating.

For *in vivo* studies, chow fed 12 w old mice were restricted from access to food for 6 h (9:00 AM – 3:00 PM) but continued to have free access to drinking water prior to harvesting livers. The treatment of mice with compound A1 was as previously described (7). Briefly, mice were fed a high fat diet (60 % kcal; D12492; Research Diets, New Brunswick, NJ, USA) starting at 5 weeks of age for 12 weeks. Administration of compound A1 or vehicle was initiated concurrently with the high fat diet. Compound A1 was prepared to a final concentration of 0.6 mg/ml in 4% DMSO and 96% of 6% hydroxypropyl-β-cyclodextrin (Sigma Aldrich) solution in sterile water. Mice were injected i.p. 5 days per week with 3 mg/kg compound A1 or the equivalent volume of vehicle (5 μl/g). Mice were fasted overnight prior to harvesting livers. Protocols for animal use, treatment and euthanasia were approved by the institutional animal care and use committee of the Harvard Medical School.

Immunoblot analysis and immunoprecipitation

Standard techniques were utilized in immunoblot analyses and immunoprecipitation assays. Cells or liver samples were washed with PBS at 4 °C and then homogenized in ice-cold RIPA buffer (50 mM Tris HCl, 150 mM NaCl, 2 mM EDTA, 0.35% NP-40, 0.5% sodium deoxycholate) containing Complete Protease Inhibitor Cocktail and PhosSTOP Phosphatase Inhibitor Cocktail Tablets (Roche, Indianapolis, IN). Cell lysates or liver homogenates were gently agitated for 30 min at 4° C and debris was removed by centrifugation (12,000 × g for 20 min at 4°C). Proteins were denatured by heating 5 min at 96°C in Laemmli buffer, separated by SDS-PAGE and transferred electrophoretically to PVDF membranes. Primary antibodies were detected using goat anti-mouse (Sigma-Aldrich) or anti-rabbit horseradish peroxidase-conjugated secondary antibodies (Bio-Rad, Hercules, CA) and visualized using enhanced chemiluminescence (GE Healthcare). Images were captured with a Bio-rad Chemidoc XRS+ equipped with a digital camera, and densitometry was performed using the histogram analysis function of Adobe Photoshop (San Jose, CA). For IRS2, the rate constant

(k) for decreases in electrophoretic mobility was calculated according to first-order kinetics using Prism 4 from the time-dependent decay of retention factor (R_f) of the IRS2 protein band in relation to a non-specific protein band (R_f = mobility of IRS2/mobility of non-specific band) in response to 1 μM compound A1.

Immunoprecipitation assays using Protein A Dynabeads were performed according to the manufacturer's instructions (Invitrogen). Briefly, 25 μl of Dynabeads were washed once with PBS and incubated (20 min at 20°C) with either rabbit IgG for pre-clearing (4 μg antibody per run) or primary antibody for precipitation. This was followed by three washes with PBS. Cell or tissue lysates containing 2 mg/ml total protein were pre-cleared for non-specific binding by incubating (1 h at 4 °C) with rabbit IgG antibody-bound Dynabeads, after which these beads were discarded and the supernatant was used to immunoprecipitate the desired protein by incubation (2 h at 4 °C) with primary antibody-bound Dynabeads. Co-immunoprecipitation of endogenous TSC2 and PC-TP was done by incubating pre-cleared lysates with PC-TP antibody-bound Dynabeads overnight at 4 °C, followed by 2 h at room temperature. IRS2 phosphorylation at residue Tyr^{911} was measured by immunoprecipitating IRS2 overnight at 4 °C followed by immunoblotting with an anti p-IRS1(Y865) antibody (Cell Signaling Technology) as described (34). Beads were then washed 5 times with RIPA buffer. Immunoprecipitated proteins were eluted and denatured by heating 5 min at 96 °C in Laemmli buffer and then subjected to immunoblot analysis.

Antibody characterization

A site-specific mouse antibody to phosphorylated IRS2 at Ser^{924} was prepared by injecting mice with the p-Ser IRS2 peptide (sequence: CEAGTRLSPPAPPLLA) coupled to keyhole limpet hemocyanin. The antibody was purified using protein G and characterized using a phosphopeptide binding assay (Fig. S3, A to C). Briefly, IRS1 and IRS2 peptides containing phosphorylated and non-phosphorylated Ser or Thr residues were purchased from Synpep (Dublin, CA). The specific Ser or Thr residue was flanked by 5–8 amino acids on either side. Wells of clear plastic 96-well plates were coated with peptides by overnight incubation at 4° C. Peptides were then exposed to various dilutions of p-IRS2(Ser^{924}) antibody for 1 h at 20° C. Plates were then incubated with a goat anti-mouse alkaline phosphatase-conjugated secondary antibody (Jackson Immunoresearch Laboratories, Inc., West Grove, PA) for 1 h at 20° C. Following the addition of a phosphatase substrate (Sigma-Aldrich), antibody binding to peptides was determined according to increases in relative light units (RLU). The antibody was further characterized by immunoblot analysis of primary hepatocytes cultured from *Irs1*$^{-/-}$/*Irs2*$^{-/-}$double knock out mice (42). Following hepatocyte isolation, cells were infected at 1–2 MOI using recombinant adenovirus for IRS2 (Ad-IRS2) for positive control (42) or GFP (Ad-GFP) for negative control (42) for 24 h, serum starved for 16 h and insulin-stimulated (10 nM for 30 min) prior to immunoblot analysis for p-IRS2(Ser^{924}) and total IRS2.

Glutathione S-transferase (GST) pulldown assay

Plasmids for the expression of recombinant GST and N-terminal tagged human GST-PC-TP (43) were utilized for GST pulldown assays as previously described (10). Recombinant GST and GST-PC-TP proteins were expressed in *Eschericia coli* BL21(DE3) by IPTG induction in 100 ml LB cultures at room temperature. GST or GST-PC-TP proteins were harvested, purified and bound to glutathione-Sepharose 4B beads (44). Beads were harvested by centrifugation (200 × g for 1 min) and washed 5 × in 1 ml ice-cold PBS. Yield and purity of proteins were assessed by Coomassie brilliant blue and Ponceau S staining. HEK 293E cells were grown to 80% confluence in 10 cm culture dishes (BD Biosciences). After washing with ice-cold PBS, cells were harvested in 2 ml RIPA buffer as described above. Lysates (1.5 mg protein/ml) were incubated with equal volumes of beads bound with recombinant

expressed GST or GST-PC-TP. In some experiments, lysates and beads bound with recombinantly expressed GST or GST-PC-TP were separately pre-incubated with compound A1 or vehicle in 0.05% DMSO for 20 m prior to mixing. After gentle mixing for 2 h at room temperature, beads were harvested by centrifugation (200 × g for 1 min at 4 °C). Beads were washed 7 × with ice-cold 1 ml RIPA buffer and then resuspended in 30 μl RIPA buffer. Beads and proteins were denatured by heating (5 min at 96 °C) in Laemmli buffer and then subjected to immunoblot analysis.

Protein stability assay

Cells were incubated in DMEM containing 100 μg/ml cycloheximide or vehicle (0.1% v/v final concentration of DMSO) at 37 °C for up to 4 h. Proteins were then harvested in ice-cold RIPA buffer and subjected to immunoblot analysis. Protein half-life ($t_{1/2}$) was calculated from the time-dependent decay of expression according to first-order kinetics using Prism 4.

mTORC2 kinase assay

The *in vitro* kinase activity of endogenous mTORC2 was measured essentially as described (15). Briefly, cells were first transfected with PC-TP, THEM2 or scrambled siRNAs and grown to 80% confluence in 10 cm plates. After 48 h, cells were washed once with ice-cold PBS and then lysed in 1 ml of lysis buffer containing 40 mM HEPES, 120 mM NaCl, 1 mM EDTA, 0.3% CHAPS {3-[(3-chloramidopropyl)-dimethylammonio]-1-propanesulfonate}, 10 mM sodium pyrophosphate tetrabasic, 10 mM β-glycerophosphate, 50 mM NaF, 0.5 mM orthovanadate, pH 7.5 plus Roche Complete Protease Inhibitor Cocktail (15, 45). Lysates were cleared of cellular debris by centrifugation (12,000 × g for 20 min at 4 °C). For mTORC2 immunoprecipitation, 1 ml of cell lysate (1.5 mg protein) was incubated with 1.5 μg anti-RICTOR antibody for 1.5 h at 4 °C. Protein G Plus/Protein A agarose beads (10 μl), prepared 1:1 (v/v) in 40 mM HEPES, 120 mM NaCl, pH 7.5 were added, and the complex was incubated for an additional 1.5 h at 4 °C. Immunoprecipitation with rabbit IgG antibody served as a control for Akt phosphorylation in the absence of mTORC2. Beads were then pelleted and washed thrice for 5 min in lysis buffer followed by twice for 5 min in mTORC2 kinase reaction buffer (25 mM HEPES, 100 mM potassium acetate, 2 mM $MgCl_2$, pH 7.5). Beads were then resuspended in 15 μl mTORC2 kinase reaction buffer. ATP (500 μM final concentration) and 500 ng of inactive Akt1 substrate (Upstate/Millipore) were added to the resuspended beads, which were then incubated for 20 min at 32 °C. The reaction was stopped by incubation at 4 °C. Samples were denatured by heating 5 min at 96 °C in Leammli buffer and subjected to immunoblot analysis.

Quantitative PCR analysis of PC-TP expression

Total mRNA was extracted from cells using TRIzol (Invitrogen) according to the manufacturer's protocol. cDNA was synthesized using the SuperScript III First-Strand Synthesis System for RT-PCR (Invitrogen). Gene expression was quantified using LightCycler FastStart DNA Master^{plus} SYBR Green I (Roche Applied Sciences) in a Lightcycler 480II (Roche Applied Sciences). Mouse L32 ribosome protein and human GAPDH were used as invariant controls (6, 11). Nucleotide sequences of oligonucleotide primers were: mouse PC-TP, forward 5′-CCAGAGTATCTCGGCACCTC-3′ / reverse 5′-ACGCTTTCACCATGTCCTTC-3′; mouse IRS2, forward 5′-GTAGTTCAGGTCGCCTCTGC-3′ / reverse 5′-CAGCTATTGGGACCACCAC-3′; human IRS2, forward 5′-CCTGCCAACACCTACGCC-3′ / reverse 5′-CTCTTTCACGATGGTGGCC-3′; human TSC2, forward 5′-TGCTCATCAACAGGCATC-3′ / reverse 5′-GCCATCACCTTCTCGATGAT-3′; human TSC1, forward 5′-GCTGCAGCATGACCGAGAG-3′ / reverse 5′-

GTGACACACCTTGTTGTTGGC-3′; mouse RPL32, forward 5′-CACCAGTCAGACCGATATGT-3′/ reverse 5′-TTCTCCGCACCCTGTTG-3′; human GAPDH, forward 5′-CCTCCCGCTTCGCTCTCT-3′ / reverse 5′-GGCGACGCAAAAGAAGATG-3′.

Quantification of phosphatidylinositol 3,4,5-trisphosphate (PIP_3)

Cellular PIP_3 concentrations were determined using a $PI(3,4,5)P_3$ Mass ELISA kit (Product No: K-2500s) from Echelon Biosciences (Salt Lake City, UT). HEK 293E cells were treated with PC-TP, THEM2, IRS2 or scrambled siRNA as described above. After 48 h, PIP_3 was extracted and quantified by ELISA according to the manufacturer's protocol using a Spectramax M5 Microplate Reader (Molecular Devices, MDS, Sunnyvale, CA). PIP_3 concentrations were determined from a standard curve using the nonlinear regression curve fit function of Prism 4.0. Each PIP_3 concentration within an experiment represents the mean of three independent determinations. IC_{50} values for inhibition of PI3K activity were calculated from decreases in PIP_3 concentrations by non-linear least square analysis using Prism 4 (GraphPad Software, La Jolla, CA).

Statistical analysis

Data are expressed as mean ± SEM of independent experiments. Means of experimental groups were compared using a two-tailed Student's *t* test or by one-way ANOVA. Differences were considered statistically significant for $P < 0.05$. For experiments comparing knockdown of PC-TP and THEM2 to the scrambled siRNA control, a Bonferroni correction was applied so that differences were considered statistically significant for $P < 0.025$.

Supplementary Material

Refer to Web version on PubMed Central for supplementary material.

Acknowledgments

The authors thank Dr. Michele Niepel for assistance with the pull-down experiments to validate PC-TP-TSC2 interactions.

Funding: This work was supported by NIH grants to DEC (DK56626 and DK48873), BDM (CA122617) TM (HL46457 and HL48743) and CU (DK080789) and by the Harvard Digestive Diseases Center (P30 DK34854). BAE is the recipient of a Ruth L. Kirschstein National Research Service Award (NRSA) (DK093195) and an American Liver Foundation Congressman John Joseph Moakley Postdoctoral Research Fellowship Award.

References and Notes

1. Wirtz KW. Phospholipid transfer proteins. Annu Rev Biochem. 1991; 60:73–99. [PubMed: 1883207]
2. de Brouwer APM, Westerman J, Kleinnijenhuis A, Bevers LE, Roelofsen B, Wirtz KWA. Clofibrate-induced relocation of phosphatidylcholine transfer protein to mitochondria in endothelial cells. Exp Cell Res. 2002; 274:100–111. [PubMed: 11855861]
3. Roderick SL, Chan WW, Agate DS, Olsen LR, Vetting MW, Rajashankar KR, Cohen DE. Structure of human phosphatidylcholine transfer protein in complex with its ligand. Nat Struct Biol. 2002; 9:507–511. [PubMed: 12055623]
4. Kang HW, Wei J, Cohen DE. PC-TP/StARD2: Of membranes and metabolism. Trends Endocrinol Metab. 2010; 21:449–456. [PubMed: 20338778]
5. Kang HW, Kanno K, Scapa EF, Cohen DE. Regulatory role for phosphatidylcholine transfer protein/StarD2 in the metabolic response to peroxisome proliferator activated receptor alpha (PPAR alpha). Biochim Biophys Acta. 2010; 1801:496–502. [PubMed: 20045742]

6. Scapa EF, Pocai A, Wu MK, Gutierrez-Juarez R, Glenz L, Kanno K, Li H, Biddinger S, Jelicks LA, Rossetti L, Cohen DE. Regulation of energy substrate utilization and hepatic insulin sensitivity by phosphatidylcholine transfer protein/StarD2. FASEB J. 2008; 22:2579–2590. [PubMed: 18347010]
7. Shishova EY, Stoll JM, Ersoy BA, Shrestha S, Scapa EF, Li YX, Niepel MW, Su Y, Jelicks LA, Stahl GL, Glicksman MA, Gutierrez-Juarez R, Cuny GD, Cohen DE. Genetic Ablation or Chemical Inhibition of Phosphatidylcholine Transfer Protein Attenuates Diet-Induced Hepatic Glucose Production. Hepatology. 2011; 54:664–674. [PubMed: 21538437]
8. Pan HJ, Agate DS, King BL, Wu MK, Roderick SL, Leiter EH, Cohen DE. A polymorphism in New Zealand inbred mouse strains that inactivates phosphatidylcholine transfer protein. FEBS Lett. 2006; 580:5953–5958. [PubMed: 17046758]
9. Dolley G, Berthier MT, Lamarche B, Despres JP, Bouchard C, Perusse L, Vohl MC. Influences of the phosphatidylcholine transfer protein gene variants on the LDL peak particle size. Atherosclerosis. 2007; 195:297–302. [PubMed: 17266964]
10. Kanno K, Wu MK, Agate DA, Fanelli BK, Wagle N, Scapa EF, Ukomadu C, Cohen DE. Interacting proteins dictate function of the minimal START domain phosphatidylcholine transfer protein/StarD2. J Biol Chem. 2007; 282:30728–30736. [PubMed: 17704541]
11. Wei J, Kang HW, Cohen DE. Thioesterase superfamily member 2 (Them2)/acyl-CoA thioesterase 13 (Acot13): a homotetrameric hotdog fold thioesterase with selectivity for long-chain fatty acyl-CoAs. Biochem J. 2009; 421:311–322. [PubMed: 19405909]
12. Kang HW, Niepel MW, Han S, Kawano Y, Cohen DE. Thioesterase superfamily member 2/acyl-CoA thioesterase 13 (Them2/Acot13) regulates hepatic lipid and glucose metabolism. FASEB J. 2012; 26:2209–2221. [PubMed: 22345407]
13. Sun XJ, Rothenberg P, Kahn CR, Backer JM, Araki E, Wilden PA, Cahill DA, Goldstein BJ, White MF. Structure of the insulin receptor substrate IRS-1 defines a unique signal transduction protein. Nature. 1991; 352:73–77. [PubMed: 1648180]
14. Bhaskar PT, Hay N. The two TORCs and Akt. Dev Cell. 2007; 12:487–502. [PubMed: 17419990]
15. Sarbassov DD, Guertin DA, Ali SM, Sabatini DM. Phosphorylation and regulation of Akt/PKB by the rictor-mTOR complex. Science. 2005; 307:1098–1101. [PubMed: 15718470]
16. Kovacic S, Soltys CL, Barr AJ, Shiojima I, Walsh K, Dyck JR. Akt activity negatively regulates phosphorylation of AMP-activated protein kinase in the heart. J Biol Chem. 2003; 278:39422–39427. [PubMed: 12890675]
17. Halse R, Rochford JJ, McCormack JG, Vandenheede JR, Hemmings BA, Yeaman SJ. Control of glycogen synthesis in cultured human muscle cells. J Biol Chem. 1999; 274:776–780. [PubMed: 9873015]
18. Manning BD, Tee AR, Logsdon MN, Blenis J, Cantley LC. Identification of the tuberous sclerosis complex-2 tumor suppressor gene product tuberin as a target of the phosphoinositide 3-kinase/akt pathway. Mol Cell. 2002; 10:151–162. [PubMed: 12150915]
19. Garami A, Zwartkruis FJ, Nobukuni T, Joaquin M, Roccio M, Stocker H, Kozma SC, Hafen E, Bos JL, Thomas G. Insulin activation of Rheb, a mediator of mTOR/S6K/4E-BP signaling, is inhibited by TSC1 and 2. Mol Cell. 2003; 11:1457–1466. [PubMed: 12820960]
20. Folkes AJ, Ahmadi K, Alderton WK, Alix S, Baker SJ, Box G, Chuckowree IS, Clarke PA, Depledge P, Eccles SA, Friedman LS, Hayes A, Hancox TC, Kugendradas A, Lensun L, Moore P, Olivero AG, Pang J, Patel S, Pergl-Wilson GH, Raynaud FI, Robson A, Saghir N, Salphati L, Sohal S, Ultsch MH, Valenti M, Wallweber HJA, Wan NC, Wiesmann C, Workman P, Zhyvoloup A, Zvelebil MJ, Shuttleworth SJ. The identification of 2-(1H-indazol-4-yl)-6-(4-methanesulfonyl-piperazin-1-ylmethyl)-4-morphol in-4-yl-thieno 3,2-d pyrimidine (GDC-0941) as a potent, selective, orally bioavailable inhibitor of class I PI3 kinase for the treatment of cancer. J Med Chem. 2008; 51:5522–5532. [PubMed: 18754654]
21. Holz MK, Ballif BA, Gygi SP, Blenis J. mTOR and S6K1 mediate assembly of the translation preinitiation complex through dynamic protein interchange and ordered phosphorylation events. Cell. 2005; 123:569–580. [PubMed: 16286006]
22. Saltiel AR, Kahn CR. Insulin signalling and the regulation of glucose and lipid metabolism. Nature. 2001; 414:799–806. [PubMed: 11742412]

23. White MF. IRS proteins and the common path to diabetes. Am J Physiol Endocrinol Metab. 2002; 283:E413–E422. [PubMed: 12169433]
24. Alessi DR, Andjelkovic M, Caudwell B, Cron P, Morrice N, Cohen P, Hemmings BA. Mechanism of activation of protein kinase B by insulin and IGF-1. EMBO J. 1996; 15:6541–6551. [PubMed: 8978681]
25. Stambolic V, Suzuki A, de la Pompa JL, Brothers GM, Mirtsos C, Sasaki T, Ruland J, Penninger JM, Siderovski DP, Mak TW. Negative regulation of PKB/Akt-dependent cell survival by the tumor suppressor PTEN. Cell. 1998; 95:29–39. [PubMed: 9778245]
26. Wang XT, McCullough KD, Franke TF, Holbrook NJ. Epidermal growth factor receptor-dependent Akt activation by oxidative stress enhances cell survival. J Biol Chem. 2000; 275:14624–14631. [PubMed: 10799549]
27. Boura-Halfon S, Zick Y. Phosphorylation of IRS proteins, insulin action, and insulin resistance. Am J Physiol Endocrinol Metab. 2009; 296:E581–E591. [PubMed: 18728222]
28. Copps KD, White MF. Regulation of insulin sensitivity by serine/threonine phosphorylation of insulin receptor substrate proteins IRS1 and IRS2. Diabetologia. 2012; 55:2565–2582. [PubMed: 22869320]
29. White MF. The insulin signalling system and the IRS proteins. Diabetologia. 1997; 40:S2–S17. [PubMed: 9248696]
30. Tee AR, Fingar DC, Manning BD, Kwiatkowski DJ, Cantley LC, Blenis J. Tuberous sclerosis complex-1 and -2 gene products function together to inhibit mammalian target of rapamycin (mTOR)-mediated downstream signaling. Proc Natl Acad Sci USA. 2002; 99:13571–13576. [PubMed: 12271141]
31. Gao XS, Zhang Y, Arrazola P, Hino O, Kobayashi T, Yeung RS, Ru BG, Pan DJ. Tsc tumour suppressor proteins antagonize amino-acid-TOR signalling. Nat Cell Biol. 2002; 4:699–704. [PubMed: 12172555]
32. Agate, DA. Doctoral dissertation. Albert Einstein College of Medicine; Bronx, NY: 2006.
33. Wu MK, Boylan MO, Cohen DE. Cloning and gene structure of rat phosphatidylcholine transfer protein, Pctp. Gene. 1999; 235:111–120. [PubMed: 10415339]
34. Wu JH, Tseng YD, Xu CF, Neubert TA, White MF, Hubbard SR. Structural and biochemical characterization of the KRLB region in insulin receptor substrate-2. Nat Struct Mol Biol. 2008; 15:251–258. [PubMed: 18278056]
35. Alvarez E, Northwood IC, Gonzalez FA, Latour DA, Seth A, Abate C, Curran T, Davis RJ. Pro-Leu-Ser/Thr-Pro is a consensus primary sequence for substrate protein phosphorylation. Characterization of the phosphorylation of c-myc and c-jun proteins by an epidermal growth factor receptor threonine 669 protein kinase. J Biol Chem. 1991; 266:15277–15285. [PubMed: 1651323]
36. Ide T, Shimano H, Yahagi N, Matsuzaka T, Nakakuki M, Yamamoto T, Nakagawa Y, Takahashi A, Suzuki H, Sone H, Toyoshima H, Fukamizu A, Yamada N. SREBPs suppress IRS-2-mediated insulin signalling in the liver. Nat Cell Biol. 2004; 6:351–357. [PubMed: 15048126]
37. Huang J, Manning BD. The TSC1-TSC2 complex: a molecular switchboard controlling cell growth. Biochem J. 2008; 412:179–190. [PubMed: 18466115]
38. Kwiatkowski DJ, Manning BD. Tuberous sclerosis: a GAP at the crossroads of multiple signaling pathways. Hum Mol Genet. 2005; 14:R251–R258. [PubMed: 16244323]
39. Benvenuto G, Li SW, Brown SJ, Braverman R, Vass WC, Cheadle JP, Halley DJJ, Sampson JR, Wienecke R, DeClue JE. The tuberous sclerosis-1 (TSC1) gene product hamartin suppresses cell growth and augments the expression of the TSC2 product tuberin by inhibiting its ubiquitination. Oncogene. 2000; 19:6306–6316. [PubMed: 11175345]
40. Dibble CC, Asara JM, Manning BD. Characterization of Rictor phosphorylation sites reveals direct regulation of mTOR complex 2 by S6K1. Mol Cell Biol. 2009; 29:5657–5670. [PubMed: 19720745]
41. Wu MK, Hyogo H, Yadav S, Novikoff PM, Cohen DE. Impaired response of biliary lipid secretion to a lithogenic diet in phosphatidylcholine transfer protein-deficient mice. J Lipid Res. 2005; 46:422–431. [PubMed: 15576839]

42. Dong XC, Copps KD, Guo SD, Li YD, Kollipara R, DePinho RA, White MF. Inactivation of hepatic Foxo1 by insulin signaling is required for adaptive nutrient homeostasis and endocrine growth regulation. Cell Metab. 2008; 8:65–76. [PubMed: 18590693]

43. Feng L, Chan WW, Roderick SL, Cohen DE. High-level expression and mutagenesis of recombinant human phosphatidylcholine transfer protein using a synthetic gene: evidence for a C-terminal membrane binding domain. Biochemistry. 2000; 39:15399–15409. [PubMed: 11112525]

44. Kanno K, Wu MK, Scapa EF, Roderick SL, Cohen DE. Structure and function of phosphatidylcholine transfer protein (PC-TP)/StarD2. Biochim Biophys Acta. 2007; 1771:654–662. [PubMed: 17499021]

45. Kim DH, Sarbassov DD, Ali SM, King JE, Latek RR, Erdjument-Bromage H, Tempst P, Sabatini DM. mTOR interacts with raptor to form a nutrient-sensitive complex that signals to the cell growth machinery. Cell. 2002; 110:163–175. [PubMed: 12150925]

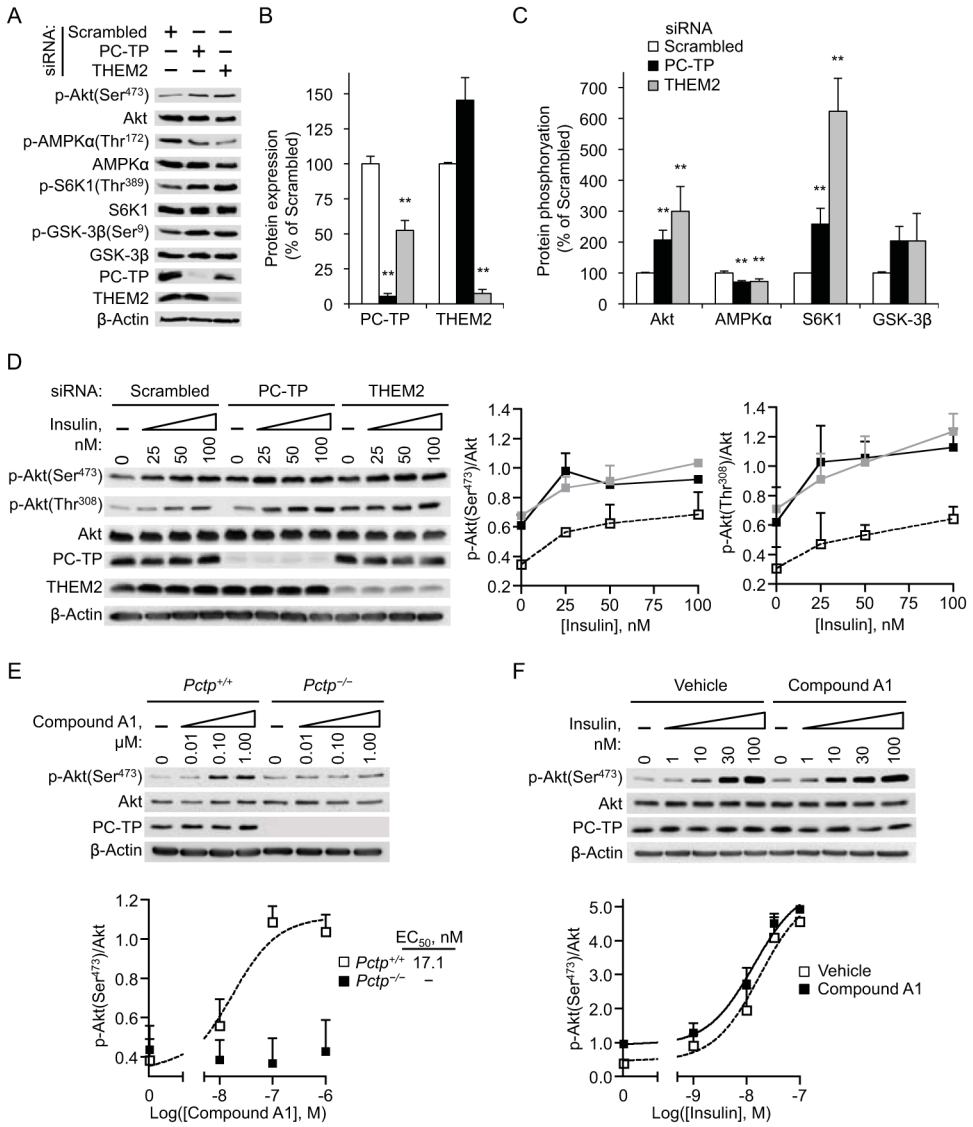

Fig. 1. Inhibition of insulin signaling by PC-TP and THEM2

(A–C) Regulation of Akt and its targets by PC-TP and THEM2 in siRNA-transfected, serum-starved HEK 293E cells. Barplots display densitometric quantification of (B) PC-TP and THEM2 and (C) protein phosphorylation. Phosphorylated proteins were normalized to total protein abundance. $^{**}P < 0.025$ compared to scrambled siRNA. (D) Insulin-induced activation of Akt after knockdown of PC-TP or THEM2 in serum-starved HEK 293E cells. Inset graphs provide densitometric quantification of p-Akt(Ser^{473}) and p-Akt(Thr^{308}) normalized to total Akt. (E) Influence of compound A1 treatment on Akt activation in primary hepatocytes. (F) Influence of compound A1 on insulin-induced phosphorylation of Akt in mouse primary hepatocytes. (E,F) Inset graphs display the densitometric quantification of p-Akt(Ser^{473}) normalized to total Akt. Immunoblots are representative of (A) 5 and (D–F) 3 independent experiments.

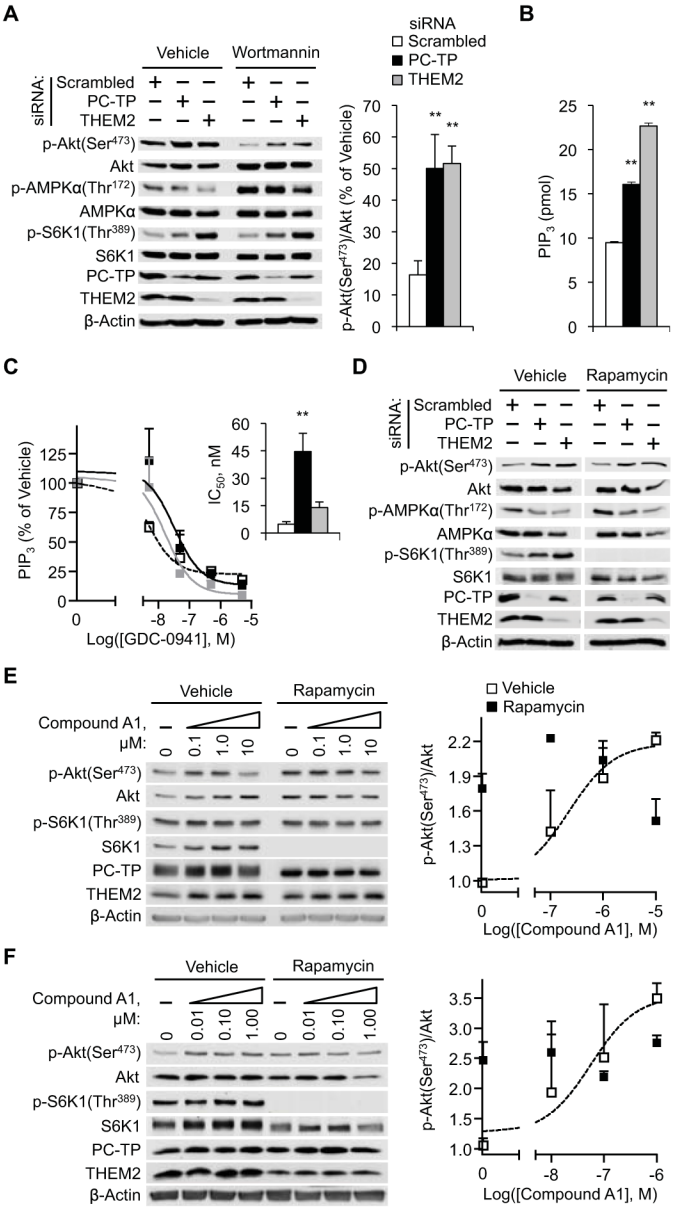

Fig. 2. Inhibition of Akt signaling by PC-TP and THEM2 depends on PI3K

(A) Influence of PC-TP and THEM2 knockdown on Akt activation in HEK 293E cells treated with wortmannin or vehicle. Inset barplot shows densitometric quantification of Akt phosphorylation normalized to total Akt. (B,C) Influence of gene knockdown on (B) cellular PIP_3 concentrations and (C) inhibition of PI3K in GDC-0941-treated cells. Inset barplot displays the IC_{50} values from 3 independent experiments. (D) Role of S6K1 in the inhibition of Akt by PC-TP and THEM2. HEK 293E cells were treated with the mTOR inhibitor rapamycin or vehicle. (E,F) Dependence of Akt activation by compound A1 on mTOR in (E) HEK 293E and (F) *Pctp*$^{+/+}$ hepatocytes. Cells were pre-incubated with rapamycin or vehicle before treatment with compound A1 in the presence of rapamycin or vehicle. Inset graphs display densitometric quantification of Akt phosphorylation normalized to total Akt. Immunoblots in each panel are representative of 3 independent experiments. $^{**}P < 0.025$ compared to scrambled siRNA.

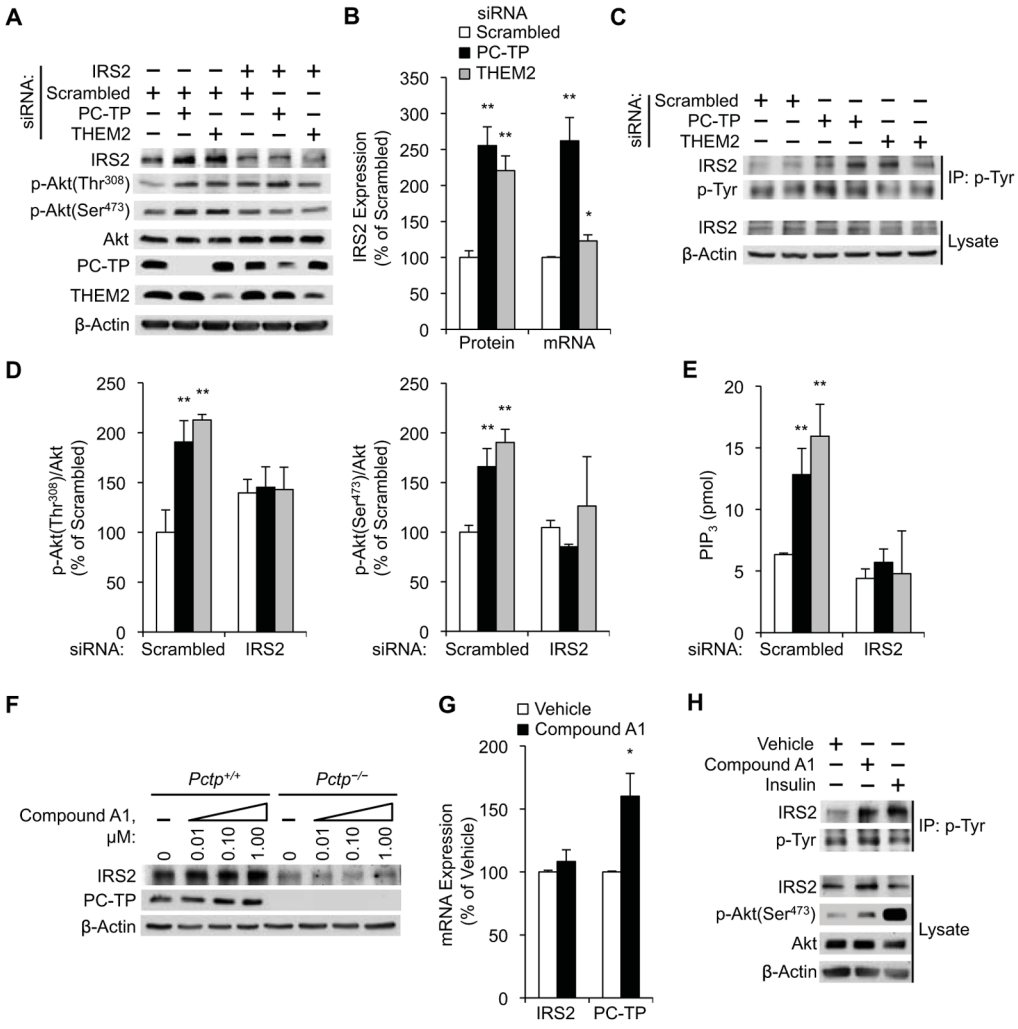

Fig. 3. PC-TP and THEM2 inhibit Akt phosphorylation through IRS2

(A) Influence of IRS2 on inhibiting Akt phosphorylation by PC-TP and THEM2 in serum starved HEK 293E cells. (B) IRS2 protein and mRNA abundance normalized to the abundance of β-Actin and GAPDH, respectively. **P* < 0.05 and ***P* < 0.025 compared to scrambled siRNA. (C) IRS2 Tyr phosphorylation (p-Tyr) as determined by immunoprecipitation. (D,E) Cells were treated as described in (A) to determine the role of IRS2 in PC-TP- and THEM2-mediated changes in (D) Akt phosphorylation (normalized to total Akt) and (E) cellular PIP_3 concentrations. ***P* < 0.025 compared to scrambled siRNA. (F) Primary hepatocytes were treated with compound A1 to determine the influence of compound A1 on IRS2 and PC-TP protein abundance. (G) Hepatocytes were treated with compound A1 or vehicle to determine the influence of compound A1 on *IRS2* and *PC-TP* mRNA abundance, which was normalized to RPL32. **P* < 0.05 compared to vehicle. (H) Influence of compound A1 treatment on Tyr phosphorylation of IRS2 in $Pctp^{+/+}$ hepatocytes compared with treatment with vehicle or insulin. Immunoblots and data are representative of (A–D) 4 and (E–F and H) 3 independent experiments.

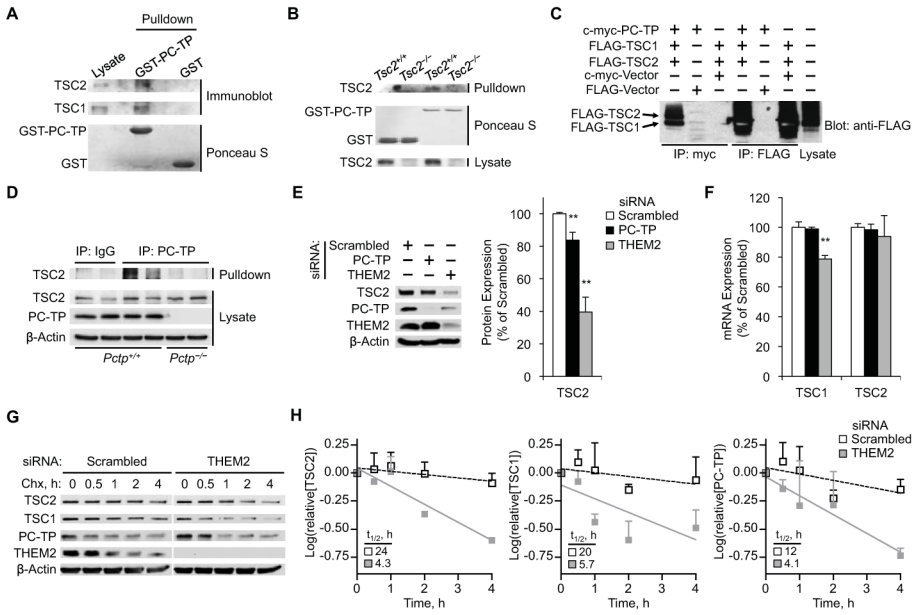

Fig. 4. PC-TP and THEM2 interact with and stabilize TSC2

Recombinant GST or GST-PC-TP fusion protein bound to glutathione-Sepharose 4B beads were used to pulldown proteins from lysates of (A) HEK 293E cells and (B) MEFs. (C) Co-immunoprecipitation of TSC1 and TSC2 by PC-TP from HEK 293E cells transfected with the indicated expression vectors. (D) Co-immunoprecipitation of endogenous TSC2 and PC-TP from *Pctp*$^{+/+}$ liver lysates. Immunoprecipitates that utilized an antibody against rabbit IgG and *Pctp*$^{-/-}$liver lysates served as controls. (E,F) Dependence of steady state abundance of TSC2 (E) protein and (F) mRNA upon PC-TP and THEM2 in serum starved HEK 293E cells. Barplots provide (E) densitometric quantification of abundance of TSC2 protein normalized to β-Actin and (F) abundance of *TSC1* and *TSC2* mRNA normalized to GAPDH. $^{**}P < 0.025$ compared to scrambled siRNA. (G) Influence of THEM2 abundance on the stability of TSC2, TSC1 and PC-TP in HEK 293E cells treated with cycloheximide (Chx). (H) Protein abundance in panel (G) normalized to β-Actin. Immunoblots and data are representative of (A–D) 3, (E) 4 and (F–G) 3 independent experiments.

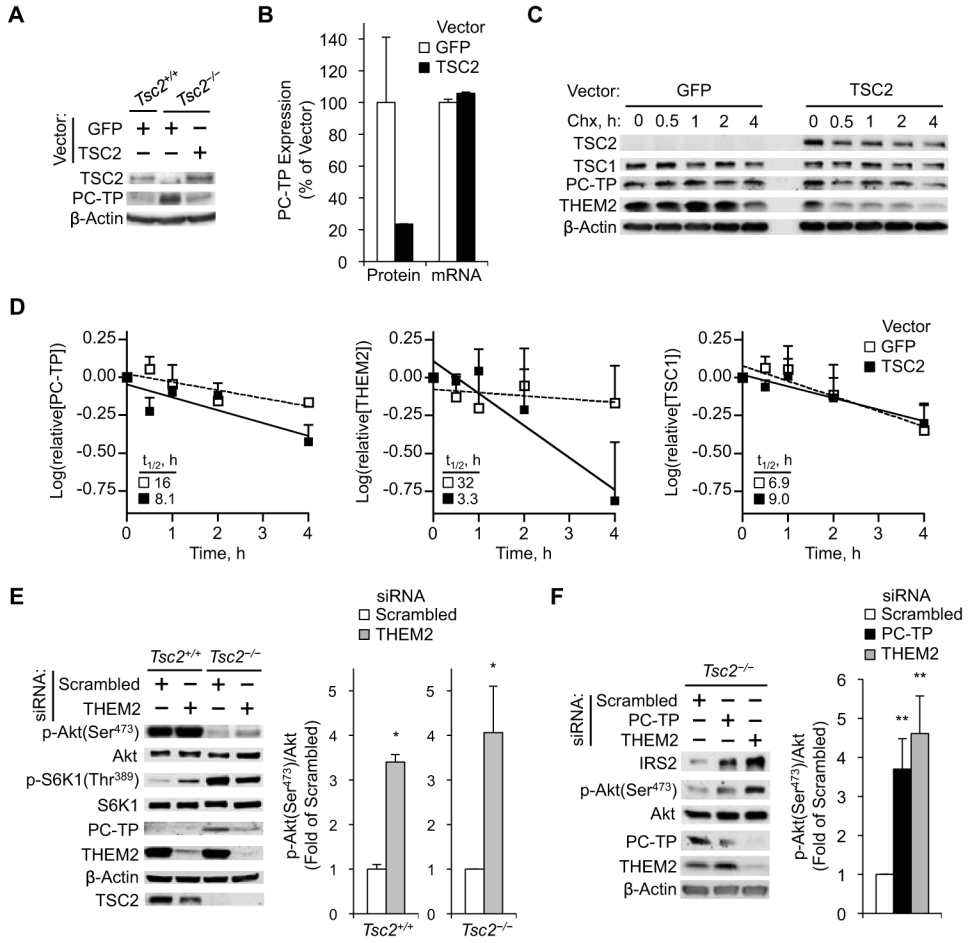

Fig. 5. Reduced PC-TP and THEM2 turnover but preserved IRS2 responsiveness in *Tsc2*$^{-/-}$MEFs

(A) Influence of TSC2 on PC-TP abundance. MEFs transfected with a green fluorescent protein (GFP) expression vector control or the vector containing TSC2 were serum starved before immunoblot analyses. (B) Densitometric quantification of steady state abundance of PC-TP protein and mRNA normalized to the abundance of β-Actin and RPL32, respectively. (C) *Tsc2*$^{-/-}$MEFs were serum starved and treated with cycloheximide (Chx). (D) Protein abundance in panel (C) quantified by densitometry and normalized to β-Actin. (E) Influence of THEM2 abundance on insulin signaling in siRNA-transfected MEFs that were serum starved before immunoblot analyses. (F) Regulation of IRS2 abundance and Akt phosphorylation by PC-TP and THEM2 in *Tsc2*$^{-/-}$MEFs after serum starvation. Inset barplots show densitometric quantification of Akt phosphorylation normalized to total Akt. **P* < 0.05 and ***P* < 0.025 compared to vehicle. Immunoblots are representative of 3 independent experiments.

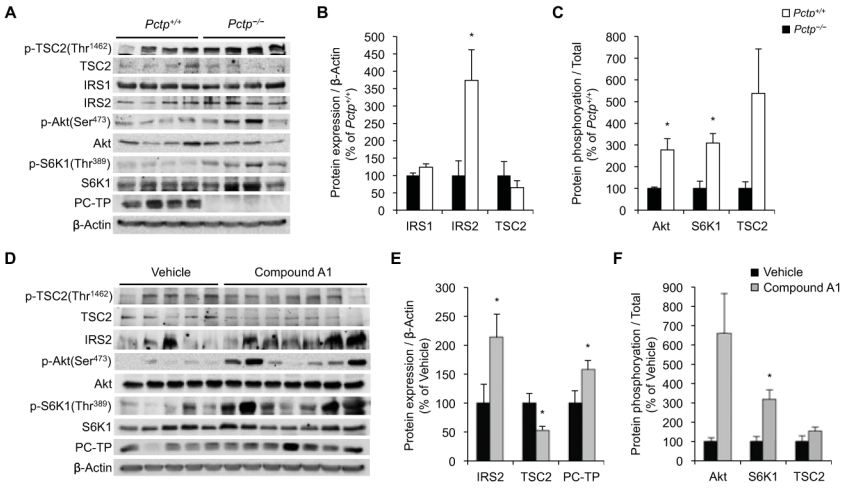

Fig. 6. Genetic ablation or pharmacological inhibition of PC-TP promotes insulin signaling *in vivo*

(A) Liver homogenates from chow diet fed $Pctp^{+/+}$ (n = 4) and $Pctp^{-/-}$(n = 4) mice were were subjected to immunoblot analyses, and bands were quantified by densitometry and normalized to (B) β-Actin or (C) total protein. **P* < 0.05 compared to $Pctp^{+/+}$. (D) Effects of compound A1 treatment on IRS2, TSC2, Akt and S6K1 in livers from $Pctp^{+/+}$ mice on high fat diets. Samples of livers from fasted mice fed a high fat diet while receiving compound A1 (n = 7) or vehicle (n = 5) as described (7) were analyzed for IRS2, p-Akt(Ser^{473}), Akt, p-S6K1(Thr^{389}), S6K1, p-TSC2(Thr^{1462}) and TSC2. Homogenates were subjected to immunoblot analyses, and bands were quantified by densitometry and normalized to (E) β-Actin or (F) total protein. **P* < 0.05 compared to vehicle.

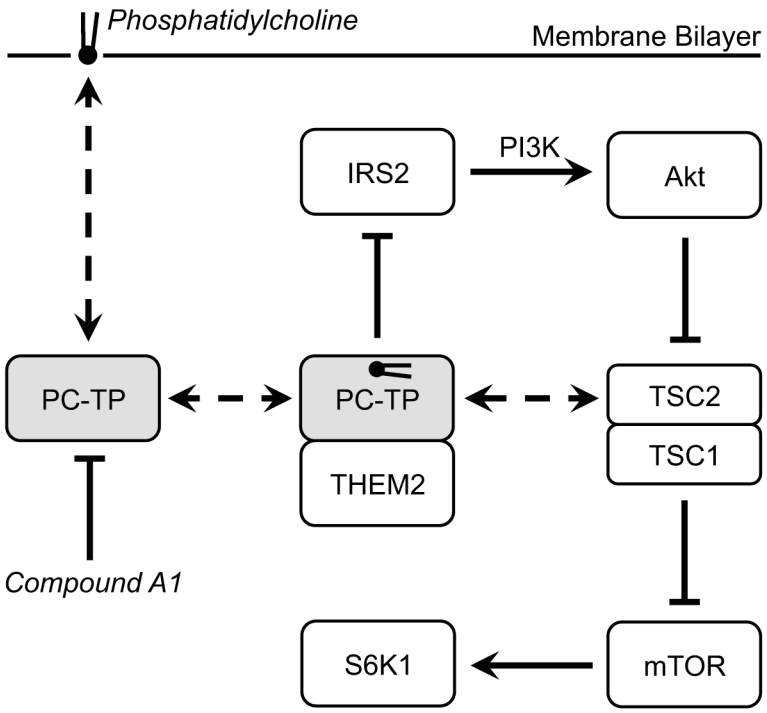

Fig. 7. Postulated mechanism by which PC-TP inhibits insulin signaling

PC-TP is proposed to serve as a sensor of changes in the molecular species of membrane phosphatidylcholines. A PC-TP-THEM2 complex limits phosphorylation of Akt by inhibiting IRS2 and that of S6K1 by stabilizing TSC1/TSC2. Dotted lines represent PC-TP binding. Arrowheads and blunt ended lines represent activating and inhibitory actions, respectively.